Applied Physics Express **9**, 032702 (2016)
http://doi.org/**10.7567/APEX.9.032702**

Optical correlation-domain reflectometry without optical frequency shifter

Makoto Shizuka, Shumpei Shimada, Neisei Hayashi, Yosuke Mizuno*, and Kentaro Nakamura

Precision and Intelligence Laboratory, Tokyo Institute of Technology, Yokohama 226-8503, Japan

*E-mail: ymizuno@sonic.pi.titech.ac.jp

Received November 12, 2015; accepted January 26, 2016; published online February 12, 2016

To achieve distributed reflectivity measurements along an optical fiber, we developed a simplified cost-effective configuration for optical correlation- (or coherence-) domain reflectometry based on a synthesized optical coherence function using sinusoidal modulation. By excluding the conventional optical heterodyne detection that accompanies the frequency shift (without using an acousto-optic modulator) and by exploiting the foot of the electrical Fresnel reflection spectrum, the electrical bandwidth required for signal processing is lowered to several megahertz. We evaluate the basic system performance and demonstrate its high-speed operation (10 ms for one scan) by tracking a moving reflection point in real time. © 2016 The Japan Society of Applied Physics

Optical reflectometry is a useful technology for monitoring the health of optical components, modules, and fiber networks, and it serves as a fundamental technique for multiplexed and distributed sensing systems[1–5] and optical coherence tomography.[6–8] To detect bad connections/splices and other reflection points along fibers under test (FUTs), two types of Fresnel-based fiber-optic reflectometry have been developed and extensively studied: optical time-domain reflectometry (OTDR)[9–13] and optical frequency-domain reflectometry (OFDR).[14–18] However, OTDR generally suffers from a relatively low spatial resolution and a low sampling rate (or a long measurement time), while OFDR commonly suffers from phase fluctuations caused by environmental disturbance. One promising method for overcoming these drawbacks is the so-called optical correlation- (or coherence-) domain reflectometry (OCDR)[19–28] exploiting a synthesized optical coherence function (SOCF),[26] which operates on the basis of correlation control of propagating light waves by modulating the laser output frequency. Two methods for frequency modulation have been implemented: sinusoidal[21–23] and stepwise modulations.[24–26] The latter includes modulations using an optical frequency comb,[27,28] which can enhance the measurement stability. Of these two frequency modulation methods, sinusoidal modulation is more suitable for cost-effective implementation.[21–23]

In conventional SOCF–OCDR systems,[21–28] the measured Fresnel spectra are shifted by several tens of megahertz by optical heterodyne detection using acousto-optic modulators (AOMs). This shift is required because otherwise the low-frequency noise from the electrical devices overlaps the electrical Fresnel spectra. If the system can be implemented without the use of an optical frequency shifter, electrical signal processing can be performed in the frequency range near DC (up to several megahertz), leading to cost reduction of relevant devices and thus of the whole system.

In this work, by excluding optical heterodyne detection, we developed a simple SOCF–OCDR configuration based on sinusoidal modulation. By exploiting the foot of the Fresnel reflection spectrum, the system was simplified with reduced cost. We further demonstrated its high-speed operation.

The experimental setup of a standard SOCF–OCDR system containing an AOM[21–23] is depicted in Fig. 1(a). The laser output is divided with a coupler; one beam is injected into an FUT, and the other beam is used as the reference light. The reflected light from the FUT is mixed with the reference light, the frequency of which is downshifted by several tens of megahertz using the AOM for optical heterodyne detection. The signal is then converted into an electrical signal with a photodetector (PD) and monitored using an electrical spectrum analyzer (ESA). Owing to optical heterodyne detection, the low-frequency noise influence of the PD and ESA can be mitigated. To achieve high-speed operation, the spectral peak power is continuously recorded using the analog output terminal of the ESA. Repetition rates of 0.1–1 Hz have been obtained by using the "peripheral component interconnect extensions for instrumentation" (PXI) platform.[23]

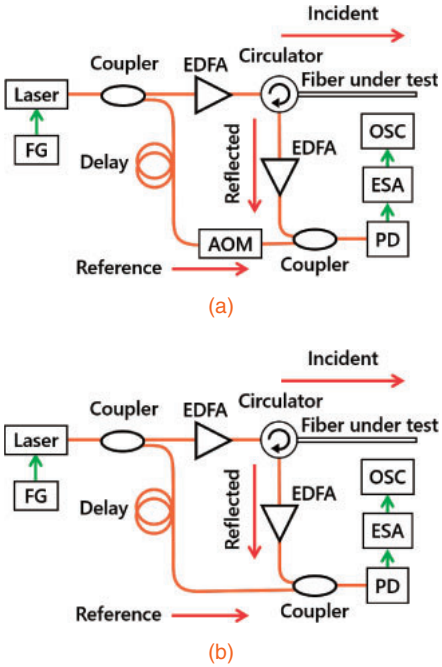

Fig. 1. Experimental setup for OCDR. (a) Conventional system and (b) new system without an AOM. EDFA: erbium-doped fiber amplifier; ESA: electrical spectrum analyzer; FG: function generator; OSC: oscilloscope; PD: photodetector.

To spatially resolve the measurement positions, we sinusoidally modulate the frequency of the laser output to form the so-called "correlation peak" in the FUT. By using the correlation peak, the reflected light generated at a specific position can be selectively observed.[26] By sweeping the modulation frequency, the correlation peak is scanned along the FUT, and thus the reflectivity can be measured in a

 © 2016 The Japan Society of Applied Physics

distributed manner. Sinusoidal frequency modulation periodically generates multiple correlation peaks, and the interval of the periodicity determines the measurement range. According to detailed calculations, the spatial resolution Δz (i.e., the 3 dB linewidth of the correlation peak) and the measurement range D are theoretically given by[29)]

$$\Delta z \cong \frac{0.76c}{\pi n \Delta f}, \quad (1)$$

$$D = \frac{c}{2nf_{\mathrm{m}}}, \quad (2)$$

respectively, where c is the light velocity in vacuum, n is the refractive index of the fiber core, Δf is the modulation amplitude, and f_{m} is the modulation frequency.

In contrast, the experimental setup of a new SOCF–OCDR system without optical heterodyne detection is shown in Fig. 1(b), which is similar to that in Fig. 1(a) except that the new system does not contain an AOM. If the optical spectrum of Fresnel reflection has a delta-function-like shape, this new configuration does not work properly. In reality, because the Fresnel spectrum has some non-negligible bandwidth (determined by the laser bandwidth),[30)] the foot of the electrical Fresnel reflection spectrum can avoid the overlap of the low-frequency noise of the PD and ESA without the use of an optical frequency shifter. In this configuration, the frequency used for measuring the optical power ranges from several hundreds of kilohertz to several megahertz. In this frequency range, the power level is lower than that at DC, and the dynamic reflectivity range is lowered. The theoretical expressions for the spatial resolution and measurement range are the same as those in the aforementioned standard SOCF–OCDR system. In this experiment, the ESA output is sent to a personal computer via an inexpensive sound card instead of the PXI platform[23)] and monitored using a virtual oscilloscope, leading to a repetition rate of >10 Hz with a less expensive system.

In the experiments below, we employed a laser diode at 1550 nm with a 3 dB bandwidth of ~1 MHz. The laser output was amplified to ~19 dBm and then injected into the FUTs. The modulation amplitude Δf was fixed at 0.75 GHz (to avoid damage to the laser), resulting in a theoretical spatial resolution of ~66 mm [see Eq. (1)]. Note that a spatial resolution of <100 μm is theoretically achievable by employing a high-speed broadband tunable laser, such as a super-structure-grating distributed Bragg reflector laser.

First, to confirm the basic operation of OCDR without optical heterodyne detection, distributed reflectivity measurements were performed using the simply structured FUT depicted in Fig. 2. A 1.0-m-long pigtail of a circulator composed of a silica single-mode fiber (SMF) was sequentially connected to 1.0- and 3.0-m-long silica SMFs using angled physical contact (APC) connectors; the end of the 3.0-m-long SMF was also kept open with an APC connector. Here, we define f_z as the central frequency of the band-pass filter of the ESA; the electrical spectral power at this frequency is selectively transmitted to an oscilloscope (OSC) to derive the reflectivity distribution along the FUT. The resolution bandwidth (RBW) and the video bandwidth (VBW) of the ESA were set to 300 and 1 kHz, respectively. The modulation frequency f_{m} was swept from 5.01 to 5.16 MHz with a repetition rate of 10 Hz, corresponding to a measurement range of approximately 20 m according to Eq. (2).

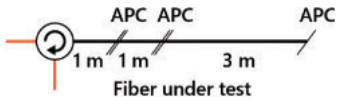

Fig. 2. Structure of the fiber under test for basic characterization.

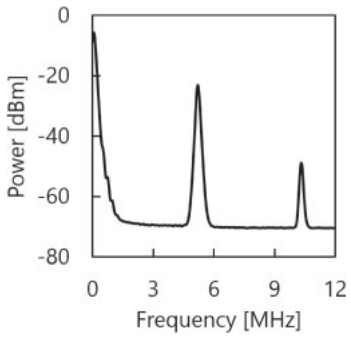

Fig. 3. Electrical spectrum measured when f_{m} was 5.1 MHz.

The measured electrical spectrum in the range from DC to 12.0 MHz (when $f_{\mathrm{m}} = 5.1$ MHz) is shown in Fig. 3. In addition to the low-frequency noise around DC, two peaks were observed at 5.1 and 10.2 MHz, which correspond to f_{m} and its second harmonic component, respectively. The reflectivity distributions obtained when $f_z = 1.2$, 2.0, and 5.0 MHz are shown in Figs. 4(a)–4(c), respectively. The relative position d was defined to be 0 at the circulator. In Figs. 4(a) and 4(b), three clear peaks were observed with reflectivities higher than −52 dB, and the locations of the peaks corresponded well to those of the APC connectors (including the open end). The relatively small peak (at $d = 0$) corresponds to the reflection at the circulator (approximately −52.5 dB). In contrast, in Fig. 4(c), no peaks were observed because of the overlap of the noise component induced by the modulation frequency f_{m}. Next, the signal-to-noise ratio (SNR), which is defined as the difference between the maximal peak power and the noise floor level, was plotted as a function of f_z (Fig. 5). When no peaks corresponding to the APC connectors were observed, the SNR was defined to be 0. The SNR deteriorated at $f_z < \sim 1$ MHz under these experimental conditions (dependent on the RBW and VBW) because of the low-frequency noise of the ESA and PD. The SNR was also reduced at f_z of around 5 MHz because of the noise caused by the laser modulation. The maximal SNR was obtained at $f_z \sim 2$ MHz.

The relationship between the peak power obtained by this method and the actual reflection power (measured using a power meter) was also investigated (Fig. 6). As the reflection power increased, the peak power increased monotonically. The nonlinear dependence was probably due to the nonlinear characteristics of the PD. Nevertheless, using this one-to-one correspondence, the actual reflection power can be inferred from the measured peak power. Note that, if different f_z values are employed, these conversion characteristics will change and need to be reinvestigated.

We subsequently performed the same measurement using another FUT with a more complicated structure (Fig. 7). The 1.0-m-long pigtail of the circulator was sequentially con-

© 2016 The Japan Society of Applied Physics

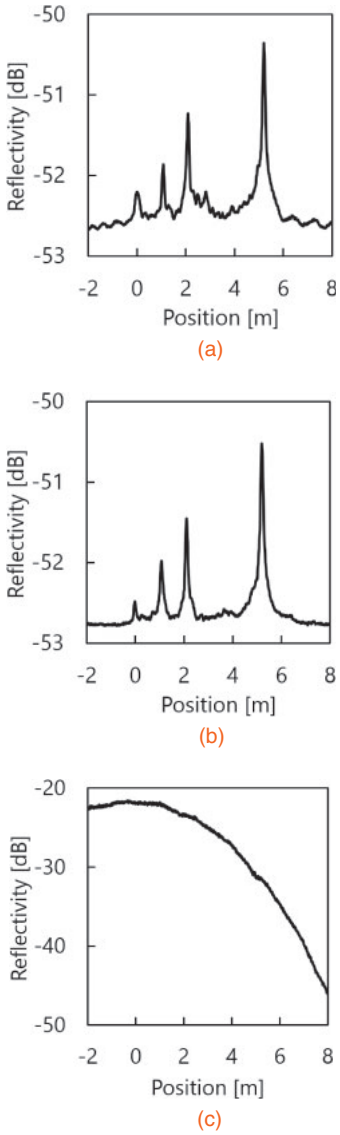

Fig. 4. Reflectivity distributions measured when f_z was (a) 1.2, (b) 2.0, and (c) 5.0 MHz.

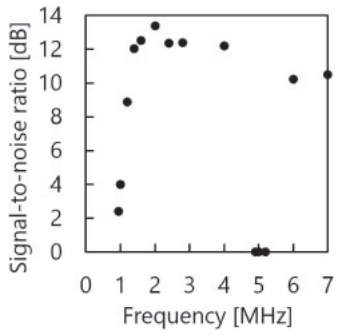

Fig. 5. SNR plotted as a function of f_z.

nected to 1.0-, 1.0-, 3.0-, and 1.0-m-long silica SMFs using APC connectors; the distal end of the FUT was also kept open with an APC connector. The modulation frequency f_m was swept from 5.01 to 5.20 MHz with a repetition rate of 10 Hz ($D \simeq 20$ m). Figure 8 shows the reflectivity distribution ($f_z = 2.0$ MHz). Five clear peaks were observed, which corresponded to the locations of the APC connectors (including the open end). A relatively small peak corresponding to the reflection at the circulator was also observed.

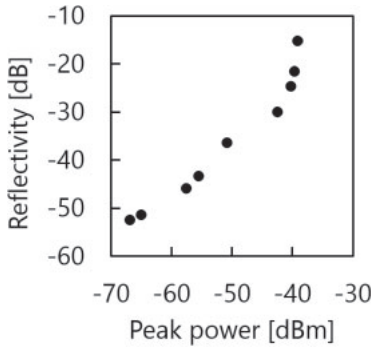

Fig. 6. Actual reflection power plotted with respect to the peak power obtained by this method.

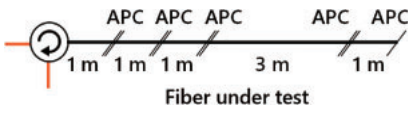

Fig. 7. Structure of the fiber under test for demonstrating multiple reflection point detection.

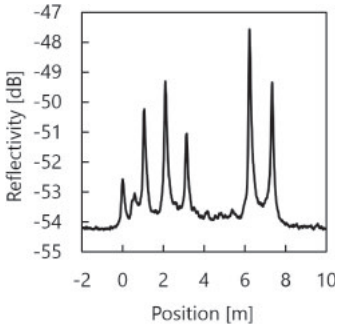

Fig. 8. Reflectivity distribution measured when f_z was 2.0 MHz.

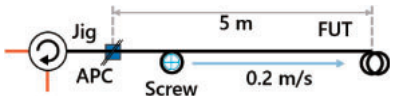

Fig. 9. Structure of the fiber under test for demonstrating high-speed operation.

Finally, the high-speed operation of this system was verified by tracking a moving reflection point. The structure of the FUT is shown in Fig. 9. Part of a 7.0-m-long silica SMF (with a 0.3-mm-thick jacket) was wound on a screw for one turn with an outer diameter of 6.4 mm (fixed on a stage), and the stage was moved along the SMF for ~3.0 m at a constant speed of 0.2 m/s. Thus, a moving reflection point can be implemented even though the reflectivity (~53 dB) is not sufficiently stable. The reflectivity distributions measured when time $t = 0$, 3.0, 6.0, and 9.0 s are shown in Fig. 10(a) (t was defined to be 0 when the screw started to move). In addition to the fixed peak at the APC connector, other peaks were clearly observed at different positions. The peak power of ~53.5 dB agreed well with the actual value (~53 dB). The peak power fluctuated within approximately ±1 dB, which could be partially attributed to the actual reflectivity fluctua-

© 2016 The Japan Society of Applied Physics

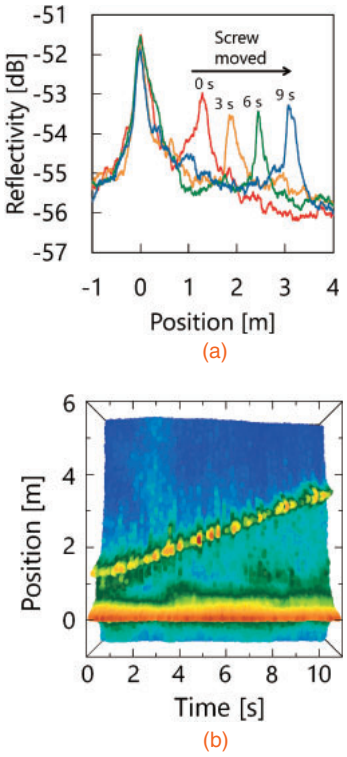

Fig. 10. (a) Reflectivity distributions measured when time $t = 0$, 3.0, 6.0, and 9.0 s. (b) Temporal variation of the measured reflectivity distribution.

tions. The temporal variation of the measured reflectivity distribution is shown in Fig. 10(b). We clearly recognize the linearly moving reflection point; from the measured data, the moving speed was calculated to be 0.19 m/s, which agrees well with the actual value of 0.2 m/s.

In conclusion, a simplified cost-effective SOCF–OCDR configuration based on sinusoidal modulation was developed by excluding conventional optical heterodyne detection, and its basic performance was evaluated. By utilizing the foot of the electrical Fresnel reflection spectrum, the electrical bandwidth required for signal processing was lowered to several megahertz. One drawback is the reduced dynamic reflectivity range. A high-speed reflectivity measurement (10 ms for acquiring one distribution) was also demonstrated by tracking a moving reflection point. Further cost reduction could be possible by replacing the ESA with an electrical circuit with an equivalent function, such as a narrow band-pass filter. We believe that this configuration will improve the convenience of the SOCF–OCDR technology for practical applications.

Acknowledgments This work was supported by JSPS KAKENHI Grant Numbers 25709032, 26630180, and 25007652, and by research grants from the Iwatani Naoji Foundation, the SCAT Foundation, and the Konica Minolta Science and Technology Foundation.

1) A. H. Hartog, A. P. Leach, and M. P. Gold, Electron. Lett. **21**, 1061 (1985).
2) P. K. C. Chan, W. Jin, J. M. Gong, and M. S. Demokan, IEEE Photonics Technol. Lett. **11**, 1470 (1999).
3) Y. Mizuno, W. Zou, Z. He, and K. Hotate, Opt. Express **16**, 12148 (2008).
4) L. Palmieri and A. Galtarossa, J. Lightwave Technol. **29**, 3178 (2011).
5) W. Zou, S. Yang, X. Long, and J. Chen, Opt. Express **23**, 512 (2015).
6) D. Huang, E. A. Swanson, C. P. Lin, J. S. Schuman, W. G. Stinson, W. Chang, M. R. Hee, T. Flotte, K. Gregory, C. A. Puliafito, and J. G. Fujimoto, Science **254**, 1178 (1991).
7) M. A. Choma, M. V. Sarunic, C. Yang, and J. A. Izatt, Opt. Express **11**, 2183 (2003).
8) Y. Kato, Y. Wada, Y. Mizuno, and K. Nakamura, Jpn. J. Appl. Phys. **53**, 07KF05 (2014).
9) M. K. Barnoski and S. M. Jensen, Appl. Opt. **15**, 2112 (1976).
10) G. P. Lees, H. H. Kee, and T. P. Newson, Electron. Lett. **33**, 1080 (1997).
11) M. Zoboli and P. Bassi, Appl. Opt. **22**, 3680 (1983).
12) P. Healey and P. Hensel, Electron. Lett. **16**, 631 (1980).
13) Q. Zhao, L. Xia, C. Wan, J. Hu, T. Jia, M. Gu, L. Zhang, L. Kang, J. Chen, X. Zhang, and P. Wu, Sci. Rep. **5**, 10441 (2015).
14) W. Eickhoff and R. Ulrich, Appl. Phys. Lett. **39**, 693 (1981).
15) D. Uttam and B. Culshaw, J. Lightwave Technol. **3**, 971 (1985).
16) B. J. Soller, D. K. Gifford, M. S. Wolfe, and M. E. Froggatt, Opt. Express **13**, 666 (2005).
17) S. Venkatesh and W. V. Sorin, J. Lightwave Technol. **11**, 1694 (1993).
18) F. Ito, X. Fan, and Y. Koshikiya, J. Lightwave Technol. **30**, 1015 (2012).
19) R. C. Youngquist, S. Carr, and D. E. N. Davies, Opt. Lett. **12**, 158 (1987).
20) E. A. Swanson, D. Huang, M. R. Hee, J. G. Fujimoto, C. P. Lin, and C. A. Puliafito, Opt. Lett. **17**, 151 (1992).
21) K. Hotate, M. Enyama, S. Yamashita, and Y. Nasu, Meas. Sci. Technol. **15**, 148 (2004).
22) Z. He, T. Tomizawa, and K. Hotate, IEICE Electron. Express **3**, 122 (2006).
23) Z. He, M. Konishi, and K. Hotate, Proc. SPIE **7004**, 70044L (2008).
24) K. Hotate and O. Kamatani, Electron. Lett. **25**, 1503 (1989).
25) Z. He and K. Hotate, J. Lightwave Technol. **20**, 1715 (2002).
26) K. Hotate, Meas. Sci. Technol. **13**, 1746 (2002).
27) Z. He, H. Takahashi, and K. Hotate, Conf. Lasers and Electro-Optics 2010 (CLEO2010), CFH4.
28) H. Takahashi, Z. He, and K. Hotate, 36th European Conf. Exhib. Optical Communication (ECOC2010), Tu.3.F.4.
29) K. Hotate and K. Kajiwara, Opt. Express **16**, 7881 (2008).
30) D. Iida and F. Ito, J. Lightwave Technol. **26**, 417 (2008).

© 2016 The Japan Society of Applied Physics